Optimization of Microbubble Concentration and Acoustic Pressure for Left Ventricular High Frame Rate EchoPIV in Patients

Voorneveld, Jason; Keijzer, Lana B.H.; Strachinaru, Mihai; Bowen, Daniel J.; Mutluer, Ferit O.; Van der Steen, Antonius F.W.; Ten Cate, Folkert; De Jong, Nico; Vos, Hendrik J.; Van den Bosch, Annemien E.

DOI
10.1109/TUFFC.2021.3066082

Publication date
2021

Document Version
Final published version

Published in
IEEE Transactions on Ultrasonics, Ferroelectrics, and Frequency Control

Citation (APA)
Voorneveld, J., Keijzer, L. B. H., Strachinaru, M., Bowen, D. J., Mutluer, F. O., Van der Steen, A. F. W., Ten Cate, F., De Jong, N., Vos, H. J., Van den Bosch, A. E., & Bosch, J. G. (2021). Optimization of Microbubble Concentration and Acoustic Pressure for Left Ventricular High Frame Rate EchoPIV in Patients. *IEEE Transactions on Ultrasonics, Ferroelectrics, and Frequency Control*, *68*(7), 2432-2443. Article 9378576. https://doi.org/10.1109/TUFFC.2021.3066082

Important note
To cite this publication, please use the final published version (if applicable).
Please check the document version above.

Optimization of Microbubble Concentration and Acoustic Pressure for Left Ventricular High Frame Rate EchoPIV in Patients

Jason Voorneveld[1], Lana B.H. Keijzer[1], Mihai Strachinaru[1,2], Daniel J. Bowen[2], Ferit O. Mutluer[2], Antonius F.W. van der Steen[1,3], Folkert ten Cate[2], Nico de Jong[1,3], Hendrik J. Vos[1,3], Annemien E. van den Bosch[2], Johan G. Bosch[1]

Abstract—High frame rate (HFR) echo-particle image velocimetry (echoPIV) is a promising tool for measuring intracardiac blood flow dynamics. In this study we investigate the optimal ultrasound contrast agent (UCA: SonoVue®) infusion rate and acoustic output to use for HFR echoPIV (PRF = 4900 Hz) in the left ventricle (LV) of patients. Three infusion rates (0.3, 0.6 and 1.2 ml/min) and five acoustic output amplitudes (by varying transmit voltage: 5V, 10V, 15V, 20V and 30V – corresponding to Mechanical Indices of 0.01, 0.02, 0.03, 0.04 and 0.06 at 60 mm depth) were tested in 20 patients admitted for symptoms of heart failure. We assess the accuracy of HFR echoPIV against pulsed wave Doppler acquisitions obtained for mitral inflow and aortic outflow. In terms of image quality, the 1.2 ml/min infusion rate provided the highest contrast-to-background (CBR) ratio (3 dB improvement over 0.3 ml/min). The highest acoustic output tested resulted in the lowest CBR. Increased acoustic output also resulted in increased microbubble disruption. For the echoPIV results, the 1.2 ml/min infusion rate provided the best vector quality and accuracy; and mid-range acoustic outputs (corresponding to 15V-20V transmit voltages) provided the best agreement with the pulsed wave Doppler. Overall, the highest infusion rate (1.2 ml/min) and mid-range acoustic output amplitudes provided the best image quality and echoPIV results.

***Index Terms*— Blood flow imaging, Contrast enhanced ultrasound, Echocardiography, Echo-particle image velocimetry, Heart failure, High frame rate imaging, Ultrafast ultrasound imaging, Ultrasound velocimetry, Vector flow imaging**

I. INTRODUCTION

BLOOD flow in the left ventricle (LV) is an important diagnostic marker for heart failure. The most widely used modality for assessing LV blood flow is echocardiography, where ultrasound Doppler is used to measure the blood velocity. However, the main limitation of ultrasound Doppler based methods is that only the velocity component in the direction of the wave propagation can be measured, the cross-beam components can only be recovered if the velocity angle is known and the beam-to-flow angle is moderate (<60° to 70° [1]). For flow in the LV, these conditions are only satisfied when measuring flow through the mitral valve and aortic outflow tract; whereas the angle of flow within the LV chamber changes over space and time.

Some echocardiographic techniques are able to estimate both the magnitude and direction of the blood velocity vectors, which we collectively name *vector flow imaging (VFI)* techniques – prominent examples include: *Transverse Oscillations*, which uses receive apodization to create a laterally oscillating field which can be used for lateral displacement estimation [2], [3]; *Vector Flow Mapping*, which calculates the lateral velocity component by post-processing colour Doppler acquisitions [4]; *Blood Speckle Tracking,* which estimates the displacement of the speckle patterns arising from red blood cell back-scatter using block-matching [5]–[7]; and *Echo-Particle Image Velocimetry* (echoPIV – also known as ultrasound image velocimetry), which also tracks speckle patterns, but those arising from ultrasound contrast agent (UCA) microbubbles which have been injected intravenously into the blood stream [8]–[11].

Clinically approved UCA are typically 1-10 μm diameter microbubbles consisting of a gas encapsulated in a lipid shell - featuring a backscatter power orders of magnitude stronger than red blood cells, allowing for improved blood opacification and SNR over native blood imaging. This SNR improvement gives echoPIV an advantage over the other VFI techniques in cardiac applications, where limited transducer aperture, large imaging depths and high velocity flows complicate measurement.

Typically, specialized pulsing schemes are used for contrast enhanced ultrasound (CEUS), such as pulse inversion (PI [12], [13]), which suppress tissue signal while retaining the

This work was supported by both ZonMw, within the Innovative Medical Devices Initiative Program under the Project 'Heart Failure and 4-D Flow'; as well as NWO within the Perspectief Program under the project 'Ultrafast Ultrasound Imaging for Extended Diagnosis and Treatment of Vascular Disease (ULTRA-X-TREME)

[1] Erasmus Medical Centre, Department of Biomedical Engineering, Rotterdam, Netherlands
[2] Erasmus Medical Centre, Department of Cardiology, Rotterdam, Netherlands
[3] Delft University of Technology, Faculty of Applied Sciences, ImPhys, Medical Imaging, Delft, Netherlands

This article has been accepted for publication in a future issue of this journal, but has not been fully edited. Content may change prior to final publication. Citation information: DOI 10.1109/TUFFC.2021.3066082, IEEE Transactions on Ultrasonics, Ferroelectrics, and Frequency Control

microbubble signal, greatly reducing clutter which would otherwise interfere with visualizing the blood pool.

Recent developments in echoPIV have used high frame rate (HFR) CEUS, utilizing plane-wave [14], [15] or diverging-wave acquisition schemes [16]–[21] instead of the focused beam-scanning schemes used on clinical scanners. This has overcome one of the key limitations of conventional echoPIV research: the severe underestimation of velocities higher than ~ 40 cm/s [22]–[24].

We have shown previously that HFR echoPIV can indeed measure the high velocity flows present in the LV *in vitro* [16] and in a patient [21]. However, the optimal UCA settings for LV VFI, such as microbubble concentration and applied acoustic pressure, have yet to be determined. It is known from conventional CEUS imaging that too low UCA concentrations result in insufficient opacification of the blood pool, while too high concentrations can result in imaging artefacts and significant attenuation, limiting visualisation of deeper regions [25], [26]. In terms of applied acoustic pressure, previous studies have shown that diverging/plane wave acquisitions should use very low acoustic pressures to prevent microbubble disruption [20], [27]–[29], but it is also expected that if acoustic pressure is too low then SNR will be insufficient for echoPIV processing.

In this study we investigate the effect of UCA infusion rate (concentration) and acoustic pressure (by varying transmit voltage) on image quality and VFI quality and peak velocity accuracy when using HFR CEUS in 20 patients.

II. Methods

A. Patient Selection and Experimental Design

After approval by the institutional review board of the Erasmus Medical Centre (NL63755.078.18), twenty patients were included who presented to the hospital with symptoms of heart failure. A wide variety of pathologies were included to test feasibility under clinically relevant imaging circumstances (details in Table 1).

Patients were first imaged with a clinical ultrasound machine (EPIQ 7, Philips Healthcare, Best, the Netherlands) and probe (X5-1, Philips Healthcare) to obtain Bmode and colour Doppler sequences of the LV in an apical 3-chamber view (Fig. 1).

TABLE I

Pathology	N	M/F	BMI	EF [%]	Age [Years]
Dilated Cardiomyopathy					
- Ischemic	5	4/1	24 (20-28)	25 (18-50)	71 (63-78)
- Non-ischemic	5	3/2	23 (20-27)	38 (20-45)	59 (19-69)
- Takotsubo	1	0/1	16	50	72
Hypertrophic Cardiomyopathy	3	1/2	29 (24-34)	45 (40-60)	51 (47-63)
Restrictive Cardiomyopathy	2	0/2	25 (20-30)	53 (45-60)	67 (64-70)
Other					
- Arrhythmia	2	2/0	26 (23-29)	43 (40-45)	40 (18-62)
- Constrictive pericarditis	1	1/0	22	70	65
Normal function	1	1/0	29	60	60

Pathological classification of patients included in study with selected details, including: number included (N), sex (M/F), body mass index (BMI), ejection fraction (EF) and Age. Metrics are shown as median (range).

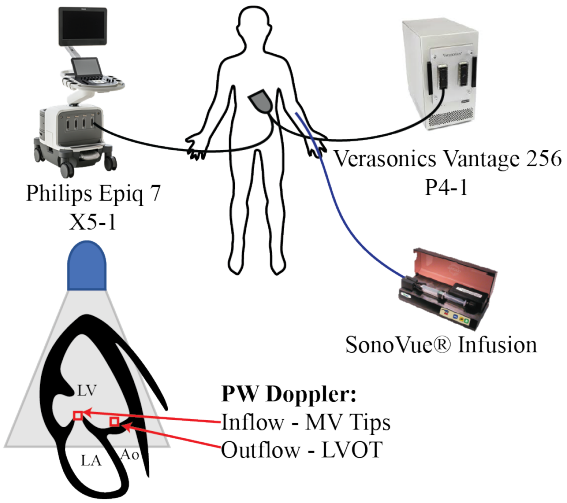

Fig. 1. Diagrammatic overview of experiment: first the patients are imaged with the clinical system (Philips), obtaining inflow and outflow PW Doppler spectra, and then the HFR CEUS acquisitions are acquired (after UCA infusion) using the research system (Verasonics).

Additionally, pulsed-wave (PW) Doppler sequences were acquired in the regions of the mitral valve (MV) tips and the left ventricular aortic outflow tract (LVOT), aligning the probe beam with the principal flow direction as best as possible.

Next, a diluted solution of UCA (SonoVue®, Bracco Imaging SpA, Milan, Italy; 5 ml SonoVue diluted with 15 ml isotonic saline) was intravenously infused using a continuous infusion pump (VueJect BR-INF 100, Bracco Imaging SpA) using the recommended infusion kit (20ml syringe, Original-Perfusor®, B.Braun, Hessen, Germany; 20G needle, Pikdare, CO, Italy; connection line: $Ø_i$=0.55 mm, L=910 mm, Sidam, MO, Italy). Three different infusion rates were tested (in order): 1.2, 0.6 and 0.3 ml/min (of the diluted UCA solution, not adjusted for weight). The arrival and stabilization of the contrast concentration was observed using the contrast mode of the clinical ultrasound machine before switching to the research system for HFR CEUS acquisitions. The HFR CEUS imaging sequences (see Section II.B) were acquired in an apical 3-chamber view using a research ultrasound system (Vantage 256, Verasonics, Kirkland, WA, USA) with a phased-array probe (P4-1, ATL). A separate line-scanning mode with real-time beamforming was used to align anatomical landmarks on the research system with those acquired with the clinical system. Five different transmit voltages (in order: 5V, 10V, 15V, 20V and 30V) were tested per UCA infusion rate. After obtaining HFR CEUS acquisitions for all transmit voltage for a given infusion rate, the infusion rate was reduced and the clinical system was used to visually confirm that the new concentration level had been reached before obtaining the next set of HFR CEUS acquisitions. Table II lists the infusion rates and transmit voltages investigated.

The whole experimental protocol took approximately 30 minutes and an extra 15 minutes if a canula needed to be inserted into the patient.

The acoustic pressures (measured using a hydrophone in water and adjusting for 0.3 dB/cm·MHz attenuation) of each transmit voltage are plotted in Fig. 2.

TABLE II

CEUS Parameters Tested				
Contrast infusion rates (in order)				
1.2 ml/min		0.6 ml/min		0.3 ml/min
Transmit Voltages (in order)				
5 V	10 V	15 V	20 V	30 V

Imaging Parameters	
Parameter	Value
PRF	4900 Hz
Transmit angles	2 (-7°, 7°)
Virtual focus radius	-47 mm
Probe	P4-1
Probe aperture	28.3 mm
CEUS mode	Pulse Inversion
Pulse type	Gaussian tapered sinusoid
Pulse centre frequency	1.5 MHz
Pulse cycles	2
Pixel size	0.31° x 308 µm
EchoPIV Parameters	
Pre-processing	
Fast-time (harmonic) filter:	4th order Butterworth (2.6-3.8 MHz)
Slow-time (wall) filter:	4th order Butterworth high-pass (100 Hz)
Boundary mask	Manually drawn (static)
PIV processing	
Number of Iterations	4
Window deformation	Bilinear
Window Size:	
- Iteration 1	10° x 10 mm (32 x 32 px)
- Iteration 2	10° x 10 mm (32 x 32 px)
- Iteration 3	5° x 5 mm (16 x 16 px)
- Iteration 4	5° x 5 mm (16 x 16 px)
Overlap	75%
- Final grid size	1.25° x 1.25 mm
Correlation averaging	(2 x angles) x (10 x frames) = 20 (~8ms)
Sub-pixel fitting	2x3 point parabolic fit
Post-processing	
Spatial smoothing	2D Gaussian (σ≈0.6 mm, extent≈4mm)
Temporal smoothing	3 ensemble moving average (~24ms)

Contrast enhanced ultrasound (CEUS) parameters tested and imaging/echoPIV parameters used in this study.

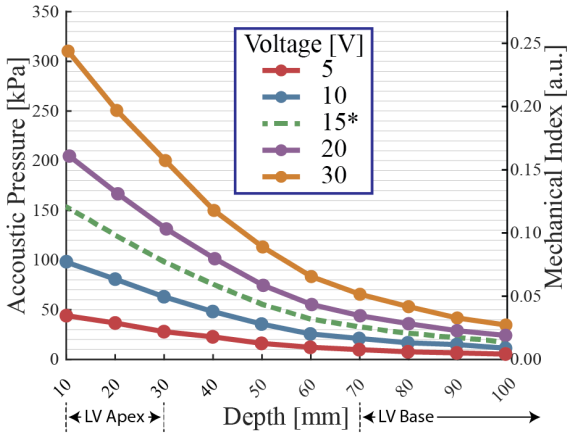

Fig. 2. Hydrophone measured pressure (left axis) and Mechanical Index (MI, right axis) as a function of transmit voltage and depth. *15V data interpolated from 10V and 20V measured data (circular markers). LV Apex and LV Base indicate the typical depths of the LV apex and base when imaging in the apical 3-chamber view. The LV base can extend up to 15 cm with larger ventricles.

B. HFR CEUS Imaging Sequence

The HFR CEUS imaging consisted of four repeated diverging-wave acquisitions: two alternating polarity transmits (pulse inversion, F_c = 1.5 MHz) at two different angles (+7°, -7°). The depth of imaging was limited to 12 cm (sufficient for normal LVs, although larger dilated LVs may require ~15 cm) and maximal obtainable pulse repetition frequency (PRF) was 4900 Hz, providing an effective frame rate of 1225 fps. A total of 2.5s was captured per acquisition, allowing for at least 2 cardiac cycles to be recorded.

Offline, saved RF data were passed through a fast-time 4th order Butterworth bandpass filter (2.6-3.8 MHz), to remove the fundamental frequency component remaining after imperfect pulse inversion cancelation. The filtered data were then beamformed onto a polar coordinate system, using the Verasonics software beamformer. A 4th order Butterworth high-pass (100 Hz ~ 3 cm/s axially) slow-time filter was then used to remove low-frequency tissue clutter.

The polar beamformed IQ data was used for echoPIV processing before performing coherent compounding (see Section II.C). For the Bmode images used in the final vector flow visualizations, coherent compounding was performed, as well as 10-frame ensemble-averaging after envelope detection – to match the frame rate of the resulting echoPIV results.

C. EchoPIV Processing

A PIV algorithm employing iterative window refinement and deformation, developed in Matlab (R2019a, MathWorks, Natick, Mass, USA), was used for velocity estimation on the beamformed polar domain data after envelope detection (further developed from [16], [18], [20]).

This PIV algorithm divided the image area into equally sized blocks with an overlap, then normalized cross-correlation (NXCC) was computed (in the frequency domain) on blocks between subsequent frames and the peak of each correlation function was used (after sub-pixel fitting) to obtain the displacement between the two frames per block. The iterative part of the algorithm attempts to reduce bias in the displacement estimation by performing the block-wise NXCC step multiple times, using the displacements calculated in the previous iteration to deform the target frame by the displacement field (thereby iteratively reducing the displacement between frames toward zero) [30]. Between iterations the window size is also reduced to increase the resolution, and further reduce bias of the calculated displacement field (Table II – PIV processing).

Instead of performing coherent compounding with the angular acquisitions, correlation compounding was used, where block-wise normalized cross-correlation was performed between like-angles and the resulting correlation maps averaged across the different angles [16]. Additionally, correlation averaging across an ensemble of 10 frames was used to further reduce noise.

Furthermore, a 2D Gaussian spatial smoothing filter and ensemble temporal moving average filter were applied to the computed velocity fields (Table II – Post-processing). Finally, the velocity data was scan converted for visualization using the vector projectile imaging technique [31]. See Fig. 3 for a diagrammatic overview of the process.

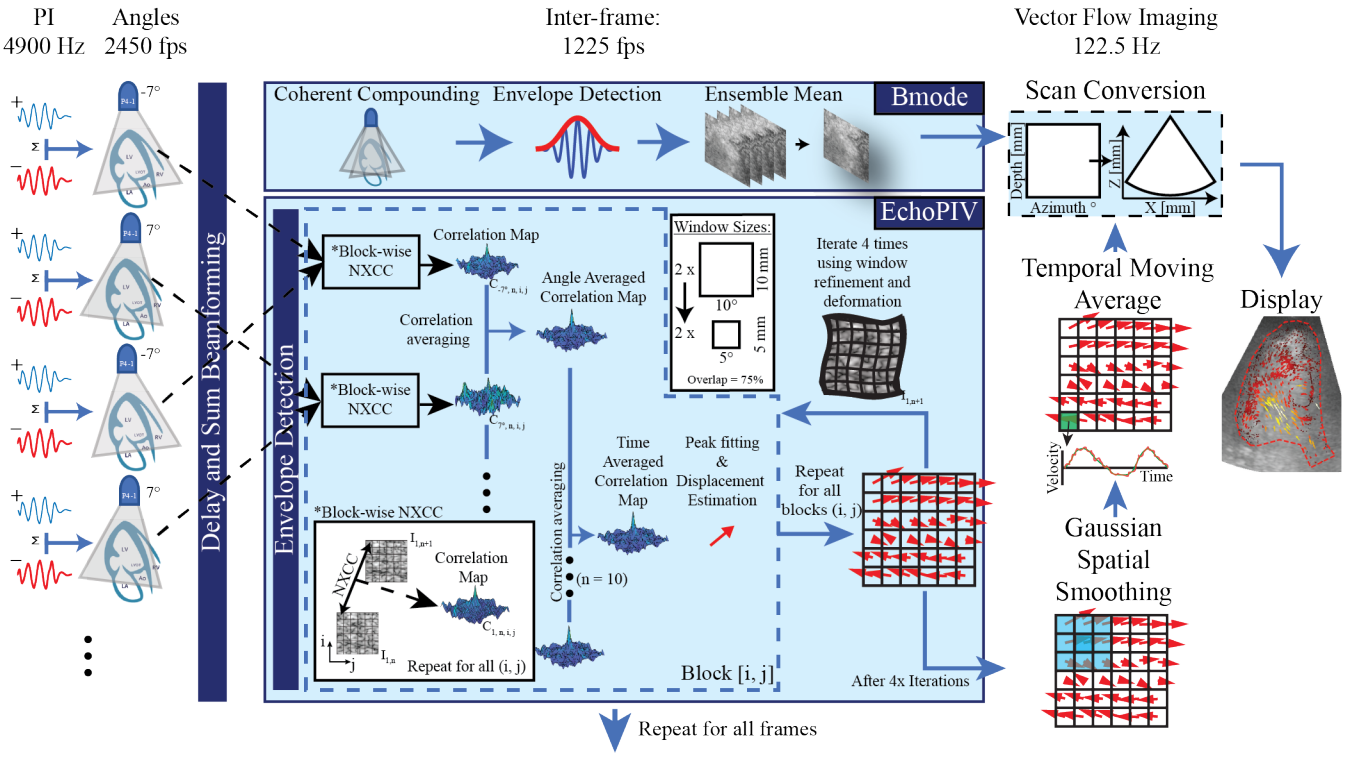

Fig. 3. Block diagram of echoPIV processing pipeline, including Bmode image processing for visualization of vector flow results. NXCC = normalized cross-correlation. See Section II.C for details.

D. *Methods of Analysis*

Four different metrics were assessed to determine which combinations of CEUS parameters were most favourable for echoPIV processing: 1) Contrast-to-background ratio (CBR), which estimates the signal power of microbubbles in relation to the unwanted background signal (be it tissue backscatter or noise); 2) microbubble disruption, where a large degree of disruption would be counter-productive for tracking the microbubbles over time; 3) qualitative assessment of the vector tracking results; and 4) accuracy of the echoPIV estimated vectors, using the peak early filling velocities from the PW Doppler spectra as a reference value. Each method is described in more detail in the following subsections.

1) *Contrast-to-Background Ratio (CBR)*

CBR was estimated as the mean signal power inside the LV cavity relative to the mean signal power of a 7.5 mm surrounding section (approximating the LV myocardium), over the whole acquisition duration. This assumes that the UCA concentration is negligible in the myocardium. CBR was calculated as follows:

$$CBR = 20\log_{10}\frac{mean(|IQ_{LV\ Cavity}|)}{mean(|IQ_{LV\ myocardium}|)} \quad (1)$$

2) *Microbubble Disruption*

Microbubble disruption was assessed by quantifying the intra-cavity signal power decrease over the first 20 frames (16 ms), using only the 1.2 ml/min contrast infusion rate. We limited the analysis to the first 20 frames (80 acquisitions, including PI and two angles) to observe the change in microbubble response at the onset of HFR imaging.

3) *Qualitative Assessment Criteria*

EchoPIV tracking quality was assessed by visually judging and scoring the vector flow visualizations according to a predetermined set of criteria (rubric – see Table III). Intra-observer and inter-observer reliability for the scoring was assessed by repeating the assessment on a subset of the patients (n=4, two non-medically trained but experienced observers: J.V. & J.G.B.) and calculating Cohens kappa statistic.

TABLE III
Qualitative Assessment Rubric

Criteria	Score 0	1	2
Clutter	Major interference with flow (> 1 position)	Minor interference with flow (1 position)	No clutter or no interference
Inflow	Not visible	Visible but noisy/underestimated (<70% PW Doppler)	Visible, smooth and in correct velocity range
Outflow	Not visible	Visible but noisy/underestimated (<70% PW Doppler)	Visible, smooth and in correct velocity range
Apical Flow	Not visible	Visible but noisy / not tracking bubbles	Visible, smooth and tracking bubble motion
Middle Flow	Not visible	Visible but noisy / not tracking bubbles	Visible, smooth and tracking bubble motion

Qualitative criteria for visual assessment of echoPIV tracking quality. There are 5 criteria each with a maximal score of 2 and a maximum total score of 10.

4) *Comparison to PW Doppler*

The ability of echoPIV to accurately estimate high velocities was assessed by regression analysis of the peak filling and ejection velocities measured using echoPIV with those measured using conventional PW Doppler. For the PW Doppler acquisitions: filling was measured between the mitral valve (MV) tips; and ejection was measured in the left ventricular outflow tract (LVOT) (See Fig. 1).

Two tracings were approximated for each PW Doppler spectrum: 1) the peak envelope of the spectrum and 2) the tracing of maximum power (see Fig. 4). The sampling area for echoPIV was adjusted to match the PW Doppler range-gate and position as closely as possible.

A single ejection / filling period was manually chosen for each echoPIV acquisition to reduce the effect of noise. If filling or ejection could not be seen in an acquisition (because of acoustic shadowing, planar misalignment or insufficient imaging depth) then the acquisition was excluded from the linear regression analysis.

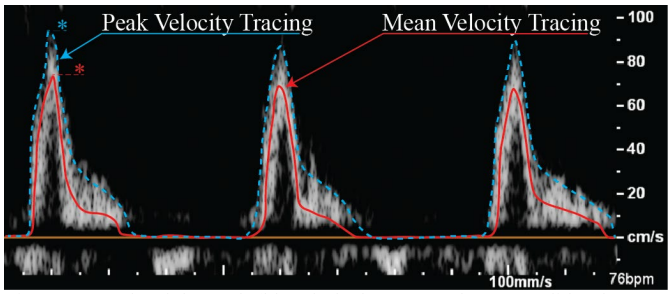

Fig. 4. Example of the peak (blue dashed curve) and mean (solid red curve) velocity tracings of the PW Doppler spectra. The maxima (*) of each over the acquired heart beats were used for the quantitative comparison with the peak echoPIV results.

E. Statistics

Data normality (of residuals) and equivariance were assessed using the Shapiro-Wilk test and Bartlett's test, respectively.

Differences in CBR (Section III.A.1) were assessed using a Welch one-way ANOVA (data residuals normally distributed but not homoscedastic) followed by post-hoc Games-Howell tests.

Microbubble disruption (Section III.A.2) was assessed using a two-way repeated measures ANOVA over time and transmit voltage.

Differences in qualitative scoring (Section III.B.1) were assessed using a Kruskal-Wallis test between concentration groups and voltages independently (data with non-normally distributed residuals but homoscedastic), followed by post-hoc Dunn's tests.

The null-hypothesis was rejected for p-values < 0.05. The mean and the bounds of the 95% confidence interval (CI) are reported in the text as: mean [95% confidence limits]

III. Results

Out of the 20 patients included in the study, one patient chose to end participation before UCA infusion. The 12 cm depth limit was sufficient for all but three patients, whose larger LVs required greater imaging depths to include the MV and LVOT; however, flow could still be observed in the LV chamber for those patients.

A. Image Quality

1) *Contrast-to-Background Ratio (CBR)*

The CBR results are tabulated in Table IV and displayed in Fig. 5. Higher microbubble infusion rates resulted in higher mean CBRs over the 2.4s acquisition period ($p<0.001$). Averaging over all infusion rates, 30V had lower CBR than 10V ($p=0.013$). Significance between voltage groups per infusion rate is shown by the horizontal bars in Fig. 5.

TABLE IV

Contrast to Background Ratio (CBR) [dB]				
	0.3 ml/min	0.6 ml/min	1.2 ml/min	All
5V	0.2 [-0.2, 0.6]	1.3 [0.6, 2.0]	3.2 [2.3, 4.0]	1.6 [1.1, 2.1]
10V	0.4 [-0.2, 1.0]	2.4 [1.5, 3.3]	4.0 [3.3, 4.8]	2.3 [1.7, 2.9]
15V	0.3 [-0.4, 1.0]	2.1 [0.9, 3.2]	3.8 [2.7, 5.0]	2.1 [1.4, 2.8]
20V	-0.1 [-1.0, 0.9]	1.5 [0.6, 2.5]	3.5 [2.3, 4.8]	1.7 [1.0, 2.4]
30V	-0.5 [-1.7, 0.6]	0.7 [-0.4, 1.9]	2.4 [1.3, 3.4]	0.9 [0.2, 1.5]
All	-0.1 [-0.3, 0.4]	1.6 [1.2, 2.0]	3.4 [2.9, 3.8]	1.7 [1.4, 2.0]

Mean [95% CI] CBRs across groups and their aggregates.

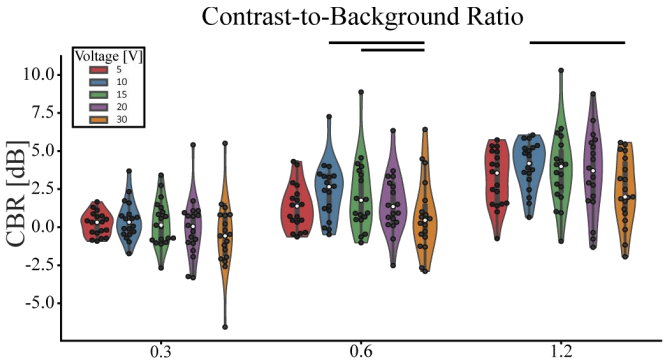

Fig. 5. CBR increases with UCA infusion rate but a transmit voltage of 10V provides the highest CBR on average. Violin plots indicate kernel density estimates of the data points (black dots). White circles indicate the median. Black horizontal bars indicate statistically significant differences. See Section III.A.1) for details.

2) *Microbubble disruption*

Higher transmit voltages resulted in more microbubble disruption ($p < 0.0001$), as is visualized by analysing the intra-cavity signal levels in the first 20 imaging frames for the 1.2ml/min infusion rate sequences (Fig. 6). After 20 frames (16 ms) the signal level had dropped by 0.6 dB [0.4 dB, 0.8 dB], 1.1 dB [0.9 dB, 1.3 dB], 1.7 dB [1.4 dB, 2.1 dB], 2.2 dB [1.9 dB, 2.6 dB] and 2.5 dB [1.9 dB, 3.1 dB] for 5V, 10V, 15V, 20V and 30V transmit voltages, respectively.

The effect of transmit voltage and UCA infusion rate on ventricular opacification and microbubble disruption is visualized in Supplementary Movie 1.

B. Vector Flow Quality

1) *Qualitative Comparison*

The qualitative scores are summarized in Table V and Fig. 7. Similar to the CBR results, increasing UCA infusion rate

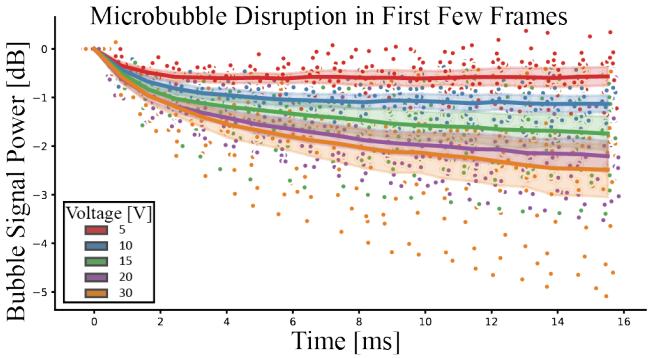

Fig. 6. Mean LV microbubble signal intensity decreased in the first 20 frames (80 acquisitions) after HFR imaging started (1.2 ml/min infusion rate). Higher transmit voltages increased the degree of signal power loss. Individual patient data are indicated with points while the lines and shaded regions indicate the mean and 95% confidence interval of each voltage group.

resulted in increasing qualitative scores (p-value <0.0001). Averaging across infusion rates, significant differences were found between: 5V and 10V (p = 0.008); 5V and 30V (p<0.001); 10V and 20V (p=0.001); 10V and 30V (p<0.0001); 15V and 20V (p=0.02); 15V and 30V (p=0.001); and 20V and 30V (p=0.002). Significance between voltage groups per infusion rate is shown by the horizontal bars in Fig. 7a.

The reliability of the qualitative scoring (Cohens kappa statistic) was 74% and 63% for intra- and inter-observer analysis, respectively (Fig. 7b). Examples of the echoPIV results using a subset of the CEUS settings are shown in Fig. 8 (animated version in Supplementary Video 2).

The mean scores for each of the criteria listed in Table III are presented as heat-maps in Supplementary Figure 1.

2) *Comparison with PW Doppler*

Only the 1.2 ml/min UCA infusion rate acquisitions are shown (Fig. 9 & Fig. 10), as lower infusion rates did not produce statistically significant regressions. Out of the 95 acquisitions using the 1.2 ml/min infusion rate, the inflow and outflow could not be seen in 13 (14 %) and 29 (31 %) acquisitions, respectively. The most common reasons for lack of visibility included planar misalignment, acoustic shadowing from the ribs or poor acoustic coupling with the skin.

TABLE V

Qualitative Vector Flow Scoring [a.u.]

	0.3 ml/min	0.6 ml/min	1.2 ml/min	All
5V	2.8 [2.0, 3.7]	4.1 [3.0, 5.2]	6.1 [4.7, 7.4]	4.3 [3.6, 5.0]
10V	4.1 [2.7, 5.5]	5.1 [3.9, 6.2]	6.7 [5.6, 7.9]	5.3 [4.6, 6.0]
15V	3.6 [2.3, 4.9]	5.0 [3.8, 6.1]	6.1 [5.0, 7.2]	4.9 [4.2, 5.6]
20V	2.5 [1.3, 3.8]	4.2 [3.1, 5.3]	5.4 [4.4, 6.5]	4.1 [3.4, 4.7]
30V	1.8 [0.7, 3.0]	2.4 [1.4, 3.5]	4.7 [3.5, 5.9]	3.0 [2.3, 3.7]
All	3.0 [2.5, 6.3]	4.1 [3.6, 4.6]	5.8 [5.3, 6.3]	4.3 [4.0, 4.6]

Mean [95% CI] vector flow quality scores across groups and their aggregates. Maximum score was 10.

Linear regressions of the maximum echoPIV velocities during inflow and outflow are plotted against the peak PW Doppler velocities for the maximum (Fig. 9) and mean (Fig. 10) spectral tracings. Overall, the comparison with the mean velocity spectral tracing produced regression slopes that were closer to unity than the maximum velocity spectral tracing. Agreement between echoPIV and PW Doppler was also stronger for inflow than outflow, with higher r^2 values, slopes and y-intercepts closer to zero. For inflow, the 15V acquisitions performed best overall, with the highest r^2 values (max tracing = 0.77, mean tracing = 0.68) and slopes (max tracing = 0.83, mean tracing = 0.99). For outflow, the 20V acquisitions performed best, with the highest r^2 (max tracing = 0.54, mean tracing = 0.51) values and slopes (max tracing = 0.74, mean tracing = 0.77).

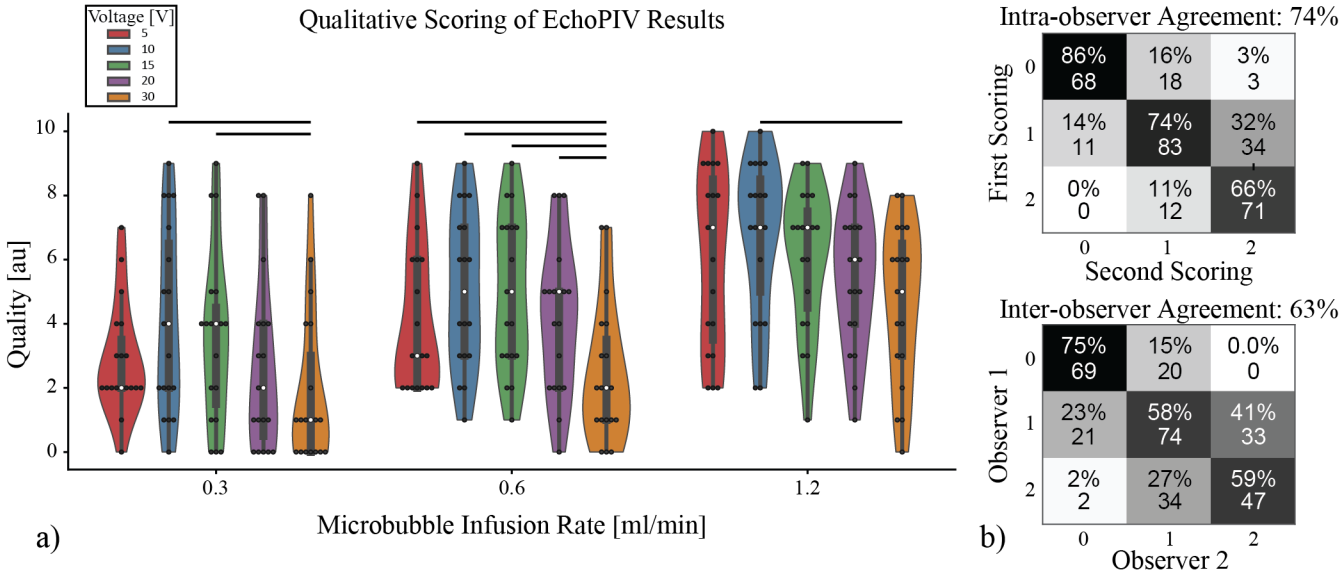

Fig. 7. Qualitative assessment of echoPIV results. **a**) scoring distribution per group, where higher concentrations scored higher on average and 30V transmit voltage scored lowest on average. Black horizontal bars indicate statistically significant differences. Violin plots indicate kernel density estimates of the data points (black dots). White circles indicate the median of each group. **b**) Confusion matrices for intra-observer and inter-observer reliability (top values indicate percentage in each bin and bottom values the count – out of 15 setting combinations x 4 patients x 5 criteria = 300).

This article has been accepted for publication in a future issue of this journal, but has not been fully edited. Content may change prior to final publication. Citation information: DOI 10.1109/TUFFC.2021.3066082, IEEE Transactions on Ultrasonics, Ferroelectrics, and Frequency Control

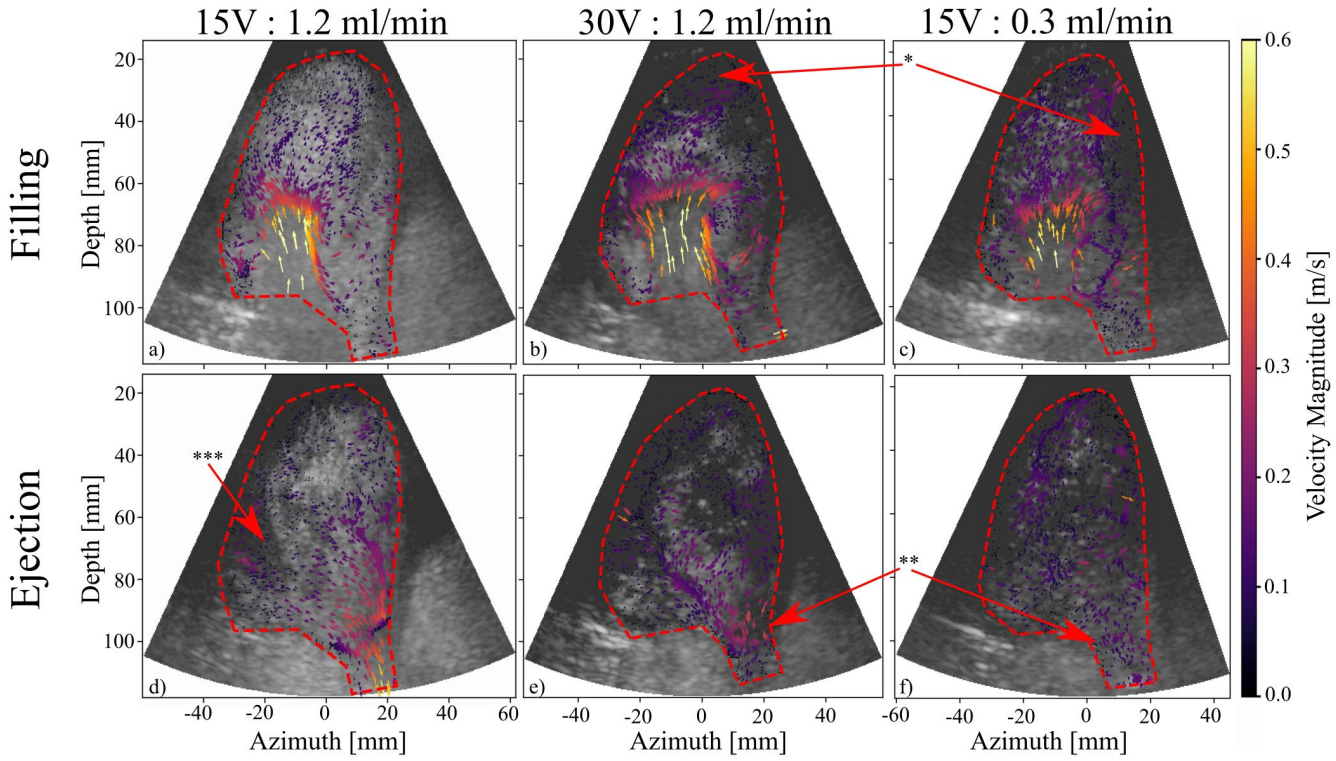

Fig. 8. Examples of echoPIV results during filling and ejection (rows) in a patient (with exemplary image quality) when using different CEUS parameters (columns). Tracking of the trans-mitral jet is similar between settings, but low signal levels are observed in the high voltage and low concentration settings (b & c: *). Ejection velocities are higher for the mid-range voltage and high infusion rate (d), than the high voltage or low infusion rate settings (e & f: **). *** papillary muscle. See Supplementary Movie 2 for animations of this figure.

IV. Discussion

We have demonstrated that HFR echoPIV is feasible in patients with heart failure due to different aetiologies, and have assessed the influence of UCA infusion rate and transmit voltage on the image and vector flow quality. We found that the highest infusion rate tested (1.2 ml/min of the 1:3 UCA dilution) was optimal for image and vector flow quality, where lower infusion rates had lower CBRs, especially in systole after a relatively long period of microbubble disruption. We also found that the lowest (5V) and highest (30V) transmit voltages performed the worst in terms of vector flow quality and accuracy.

A. Feasibility

Out of the 19 patients that obtained HFR CEUS recordings, 14 obtained at least one acquisition with qualitative scores higher than 5 out of 10 (Fig. 11). Of the five patients that did not achieve at least a 5 out of 10 score, no particular pathology occurred more often than the others. The main reasons for the low scoring in these patients was low SNR in the basal region (resulting in noisy inflow and outflow vectors), planar misalignment or entire regions of the LV being hidden due to rib shadowing or clutter.

We also found that inflow was visible more often than outflow (Fig 9, Fig 10 and Supplementary Figure 1). The reason for the lower visibility of outflow in this study is not certain but may be due to: 1) angle of the outflow tract when viewed in the apical 3-chamber view (outflow is angled out-of-plane and thus underestimated or untracked); 2) the deeper placement of the LVOT in the apical 3-chamber view than the inflow jet, resulting in lower SNR and resolution; and 3) the small diameter of the LVOT (relative to the LV in the region of the inflow jet) which would result in higher side-lobes levels from the surrounding vessel/tissue (increased clutter) and would also complicate aligning the scan plane to the central cross-section of the outflow tract – exacerbating point 1).

These view issues could likely have been avoided if real-time feedback on the HFR CEUS image quality could be obtained. In this study, the sonographer was not able to view the resulting HFR recordings after acquisition due to the excessive image reconstruction time. Beamforming on Graphical Processing Units (GPUs) and/or data decimation may provide the image reconstruction rates required to display the captured HFR CEUS data immediately after acquisition. Expanding to 3D VFI would also provide a potential solution to the out-of-plane flow issues [7], [32].

B. Image Quality

Higher infusion rates resulted in higher CBR on average over the whole acquisition period (Fig. 5). The highest transmit voltage (30V) had the lowest CBR, which can be attributed to 1) higher tissue intensity caused by non-linear propagation, reducing the effectiveness of the pulse-inversion technique for selectively suppressing tissue back-scatter; and 2) increased microbubble disruption (Fig. 6).

Other HFR CEUS studies have also shown similar trends between acoustic pressure (transmit voltage) and microbubble disruption when using diverging/plane wave imaging, *in vitro* [28], [29], [33] and *in vivo* in the abdominal aorta [20].

This article has been accepted for publication in a future issue of this journal, but has not been fully edited. Content may change prior to final publication. Citation information: DOI 10.1109/TUFFC.2021.3066082, IEEE Transactions on Ultrasonics, Ferroelectrics, and Frequency Control

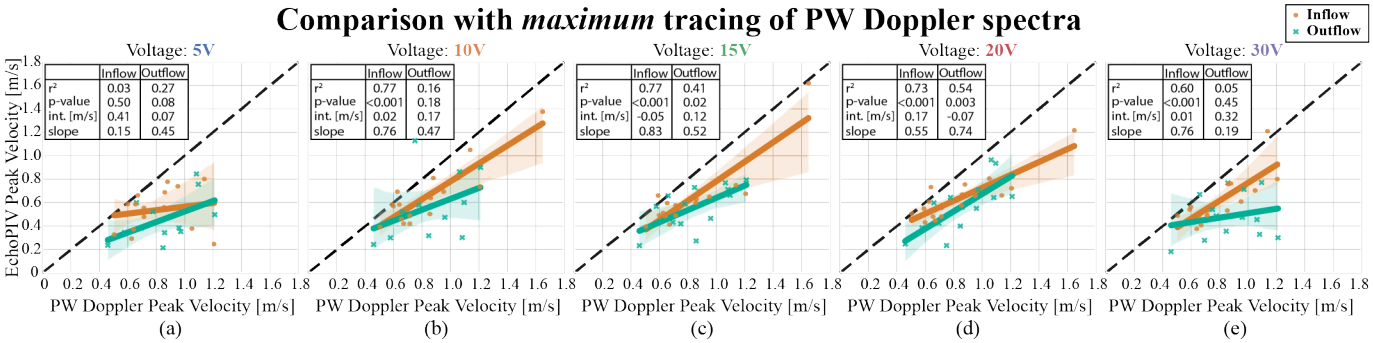

Fig. 9. Regressions of maximum echoPIV and the peak *maximum*-tracing of the PW Doppler spectra for inflow (orange circles) through the MV and outflow (cyan crosses) through the LVOT for increasing transmit voltage (a-e). Measured at 1.2ml/min infusion rate, the only infusion rate with statistically significant regressions. It can be seen that echoPIV underestimates the maximum velocities compared with spectral Doppler. Observations where inflow or outflow were not visible in the echoPIV acquisitions were excluded. Shaded area indicates 95% confidence interval.

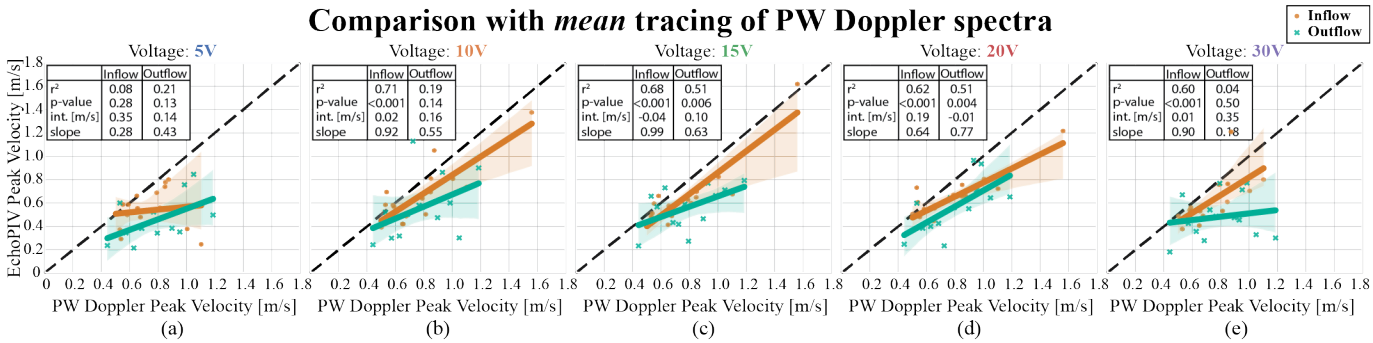

Fig. 10. Regressions of maximum echoPIV and the peak *mean*-tracing of the PW Doppler spectra for inflow (orange circles) through the MV and outflow (cyan crosses) through the LVOT for increasing transmit voltage (a-e). Better agreement is observed between echoPIV and the mean velocities in the sample volume of the PW spectra than with the maximum tracing (Fig. 9). Measured at 1.2ml/min infusion rate, the only infusion rate with statistically significant regressions. Observations where inflow or outflow were not visible in the echoPIV acquisitions were excluded. Shaded area indicates 95% confidence interval.

In conventional (line-scanning based imaging) echoPIV the reported UCA dosage varies between 0.01 ml/min and 6 ml/min for continuous infusion [34]–[36], and a consistent 0.1-0.2 ml for bolus administration [22], [23], [37]–[39]. The reported MI values used in conventional echoPIV studies are much higher (MI = 0.1 - 0.7) than those used in HFR echoPIV.

In order to perform echoPIV, which involves tracking the microbubble intensities over time, it is necessary to maximize CBR while minimizing microbubble disruption. For this purpose, we found that the highest infusion rate investigated (1.2 ml/min) and a relatively low transmit voltage (10 – 15V) was optimal. However, the optimal transmit voltage will likely vary between patients and imaging views, so it is better to preview the beamformed HFR CEUS sequence after acquisition to visually verify that CBR is sufficient while still minimizing microbubble disruption.

C. Vector Flow Quality

Similar to image quality, higher UCA infusion rates resulted in better quality velocity estimation results both qualitatively (III.B.1) and quantitatively (III.B.2). We also see that the highest transmit voltage (30V) performed the worst qualitatively, with high clutter levels which often interfered with the flow tracking. The optimal transmit voltages found were between 10V and 20V, with 10V performing best in the qualitative scoring overall.

In the echoPIV and PW Doppler derived maximum velocity comparison (during inflow and outflow), we found that the 0.3 ml/min and 0.6 ml/min concentrations produced no significant linear relationships, indicating inconsistent echoPIV accuracy using these infusion rates. For the 1.2 ml/min infusion rate, we found that the 5V acquisitions resulted in poor accuracy, despite very low clutter levels, indicating that CBR was an issue. For the 30V transmit, although clutter levels were high, we found good agreement with the PW Doppler traces for inflow but not for outflow. This discrepancy is likely due to microbubble disruption, as during filling the microbubbles are replenished and tracking is improved by high CBR; whereas during outflow significant microbubble disruption has already occurred and poor CBR is available for tracking. Another factor worth considering is the higher clutter levels observed in the 30V acquisitions, where high side-lobe levels from surrounding tissue interfere with the flow signal in the outflow tract.

Overall, the 15V and 20V acquisitions performed best in the PW Doppler comparison, where the 10V resulted in a non-significant regression for outflow. We found echoPIV underestimated peak velocities increasingly with velocity magnitude (regression slopes < 1.0; Fig. 9), similar to the findings of Nyrnes *et al.* (2020) when using blood speckle tracking [5]. Underestimation is expected as echoPIV is a block-matching technique (similar to blood speckle tracking) that estimates the bulk displacement present in the interrogation kernel, which for non-uniform flow will always be lower in magnitude than the peak displacement present in the kernel. If we instead compare the peak echoPIV velocities to the peak PW Doppler velocities obtained from the mean velocity tracing of

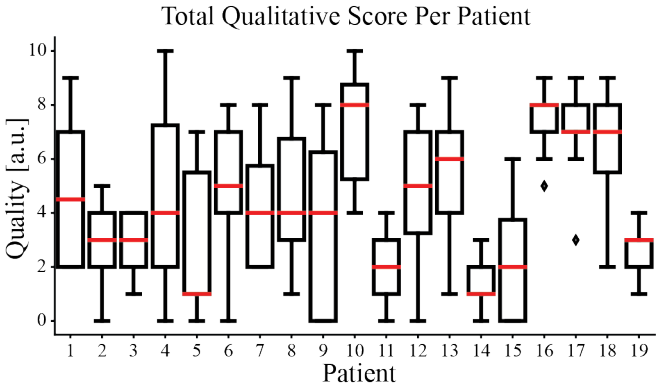

Fig. 11. Total score obtained per patient for the qualitative assessment. Note that one patient is missing due to voluntary withdrawal. Red lines indicate median, boxes extend to 25th and 75th percentiles and whiskers indicate the range excluding samples (♦) outside of 1.5 times the interquartile range.

the Doppler spectrum (Fig. 10) then the agreement is much stronger, as expected.

In our previous work [16], where we compared HFR echoPIV with optical PIV in a dynamic LV *in vitro* model, we found that echoPIV achieved normalized root-mean-squared errors (NRMSE) of 16% for the high velocities (> 30 cm/s) present in the trans-mitral filling jet. In that study we were also able to assess the similarity in flow patterns, which was good for the high energy flow patterns. Additionally, we have compared HFR echoPIV with 4D-Flow MRI in abdominal aortic flow quantification in healthy volunteers [18], also finding good agreement between the two modalities with peak velocity differences ranging between 8.5% and 17%. In that previous study we found that the lowest UCA bolus concentration was optimal; however, this conclusion was based on optimization of systolic VFI only, whereas further investigation [20] found that higher bolus concentrations were favourable during cardiac phases with less UCA replenishment, where microbubble disruption was more prevalent – similar to the findings of this study.

D. Limitations

While great care was taken to ensure that the same view was preserved between acquisitions, perfect alignment was impossible. Thus, it should be kept in mind that some of the measurement variation can be attributed to variation in imaging plane (caused by probe placement, probe motion and breathing motion). This especially applies to the comparison with PW Doppler, which was obtained with the clinical scanner before contrast infusion. In an effort to minimize view changes, we structured the acquisition protocol such that the probe only had to be removed and replaced between infusion rate changes (to check that the new UCA concentration had been reached with the clinical ultrasound system).

It is still unclear if infusion rates higher than 1.2ml/min would have provided better image and vector flow quality, as they were not tested. However, too high concentrations are known from clinical CEUS measurements to cause acoustic shadowing and non-linear propagation artefacts [25], [26], which are expected to degrade tracking quality.

The current study had a depth limit of 12 cm; however, this was only due to our fixed PRF implementation, which was used to keep the frame rate the same for all acquisitions. In future the PRF can be linked to the maximum depth of interest (based on the two-way transit time).

E. Future Improvements

While feasibility was high in this study, it could have been further improved if immediate feed-back on HFR CEUS image quality was provided to the sonographer. This would allow for bad image views to be discarded and re-captured. Increasing the beamforming speed using GPUs and/or data decimation could solve this issue in future.

Validation of flow features was not possible in this study as PW Doppler was obtained in only two points in the LV. Comparison with 4D Flow MRI would be a possible next step, allowing for flow comparison over the whole image slice.

Acquiring a full-field Eulerian velocity field allows for calculation of many relevant parameters, such as vorticity [22], [34], [39], [40], kinetic energy (dissipation) [7], and relative pressure gradients [41]. It is also possible to perform particle displacement analyses using these flow fields to simulate parameters such as particle residence time and washout period [42], [43]. The potential of using echoPIV for assessment of these parameters should be studied and validated in future work.

In this study we used only two angles for coherent compounding, in an effort to reduce the amount of scatterer motion present between angles. However, the tilt and number of angles used was not systematically optimized and may offer future improvements.

V. Conclusion

We have shown that HFR echoPIV is feasible and that it can provide estimates of the high filling and ejection velocities in the left ventricle that are consistent with PW Doppler. High UCA infusion rates provided better image quality (higher CBR) and flow tracking, with the highest infusion rate of 1.2 ml/min (of a 1:3 UCA dilution) performing best overall. Low-to-medium (10V-20V) transmit voltages performed best overall, where the lowest (5V) and highest (30V) had issues with SNR and clutter / microbubble disruption, respectively. However, these settings only provide a good starting point for optimization, where real-time feedback on the acquisition image quality should be used for further fine-tuning per patient and/or imaging view.

Acknowledgment

The authors thank Robert Beurskens, Frits Mastik and Gerard van Burken for technical assistance during the development of the HFR CEUS sequences, and Jeffrey Goei for assistance in planning the experiments.

References

[1] P. Tortoli, M. Lenge, D. Righi, G. Ciuti, H. Liebgott, and S. Ricci, "Comparison of Carotid Artery Blood Velocity Measurements by Vector and Standard Doppler Approaches," *Ultrasound Med. Biol.*, vol. 41, no. 5, pp. 1354–1362, May 2015, doi: 10.1016/j.ultrasmedbio.2015.01.008.

[2] S. Holbek *et al.*, "Real-time 2-d phased array vector flow imaging," *IEEE Trans. Ultrason. Ferroelectr. Freq. Control*, vol. 65, no. 7, pp. 1205–1213, 2018, doi: 10.1109/TUFFC.2018.2838518.

[3] K. Hansen, K. Juul, H. Møller-Sørensen, J. Nilsson, J. Jensen, and M. Nielsen, "Pediatric Transthoracic Cardiac Vector Flow Imaging – A Preliminary Pictorial Study," *Ultrasound Int. Open*, vol. 05, no. 01, pp. E20–E26, Jan. 2019, doi: 10.1055/a-0656-5430.

[4] K. C. Assi *et al.*, "Intraventricular vector flow mapping - A Doppler-based regularized problem with automatic model selection," *Phys. Med. Biol.*, vol. 62, no. 17, pp. 7131–7147, 2017, doi: 10.1088/1361-6560/aa7fe7.

[5] S. A. Nyrnes, S. Fadnes, M. S. Wigen, L. Mertens, and L. Lovstakken, "Blood Speckle-Tracking Based on High–Frame Rate Ultrasound Imaging in Pediatric Cardiology," *J. Am. Soc. Echocardiogr.*, vol. 33, no. 4, pp. 493-503.e5, Apr. 2020, doi: 10.1016/j.echo.2019.11.003.

[6] S. Fadnes, M. S. Wigen, S. A. Nyrnes, and L. Lovstakken, "In Vivo Intracardiac Vector Flow Imaging Using Phased Array Transducers for Pediatric Cardiology," *IEEE Trans. Ultrason. Ferroelectr. Freq. Control*, vol. 64, no. 9, pp. 1318–1326, Sep. 2017, doi: 10.1109/TUFFC.2017.2689799.

[7] M. S. Wigen *et al.*, "4D Intracardiac Ultrasound Vector Flow Imaging -Feasibility and Comparison to Phase-Contrast MRI," *IEEE Trans. Med. Imaging*, no. c, 2018, doi: 10.1109/TMI.2018.2844552.

[8] H. J. Vos *et al.*, "Contrast-Enhanced High-Frame-Rate Ultrasound Imaging of Flow Patterns in Cardiac Chambers and Deep Vessels," *Ultrasound Med. Biol.*, vol. 46, no. 11, pp. 2875–2890, Nov. 2020, doi: 10.1016/j.ultrasmedbio.2020.07.022.

[9] C. Poelma, "Ultrasound Imaging Velocimetry: a review," *Exp. Fluids*, vol. 58, no. 1, p. 3, Jan. 2017, doi: 10.1007/s00348-016-2283-9.

[10] D. Garcia, "Introduction to speckle tracking in cardiac ultrasound imaging," *Handb. Speckle Filter. Track. Cardiovasc. Ultrasound Imaging Video*, pp. 571–598, 2018, doi: 10.1049/pbhe013e_ch26.

[11] D. Mele *et al.*, "Intracardiac Flow Analysis: Techniques and Potential Clinical Applications," *J. Am. Soc. Echocardiogr.*, 2019, doi: 10.1016/j.echo.2018.10.018.

[12] J. Hwang and D. Simpson, "Two pulse technique for ultrasonic harmonic imaging," US5951478A, 1999.

[13] C. S. Chapman and J. C. Lazenby, "Ultrasound imaging system employing phase inversion subtraction to enhance the image," US5632277A, 1997.

[14] C. H. Leow, E. Bazigou, R. J. Eckersley, A. C. H. Yu, P. D. Weinberg, and M.-X. Tang, "Flow Velocity Mapping Using Contrast Enhanced High-Frame-Rate Plane Wave Ultrasound and Image Tracking: Methods and Initial in Vitro and in Vivo Evaluation," *Ultrasound Med. Biol.*, vol. 41, no. 11, pp. 2913–2925, Nov. 2015, doi: 10.1016/j.ultrasmedbio.2015.06.012.

[15] C. H. Leow and M.-X. Tang, "Spatio-Temporal Flow and Wall Shear Stress Mapping Based on Incoherent Ensemble-Correlation of Ultrafast Contrast Enhanced Ultrasound Images," *Ultrasound Med. Biol.*, vol. 44, no. 1, pp. 134–152, Jan. 2018, doi: 10.1016/j.ultrasmedbio.2017.08.930.

[16] J. Voorneveld *et al.*, "High Frame Rate Ultrasound Particle Image Velocimetry for Estimating High Velocity Flow Patterns in the Left Ventricle," *IEEE Trans. Ultrason. Ferroelectr. Freq. Control*, vol. 65, no. 12, pp. 2222–2232, Dec. 2018, doi: 10.1109/TUFFC.2017.2786340.

[17] M. E. G. Toulemonde *et al.*, "High Frame-Rate Contrast Echocardiography: In-Human Demonstration," *JACC Cardiovasc. Imaging*, vol. 11, no. 6, pp. 923–924, 2018, doi: 10.1016/j.jcmg.2017.09.011.

[18] S. Engelhard *et al.*, "High-Frame-Rate Contrast-enhanced US Particle Image Velocimetry in the Abdominal Aorta: First Human Results," *Radiology*, vol. 289, no. 1, pp. 119–125, Oct. 2018, doi: 10.1148/radiol.2018172979.

[19] L. Nie, D. M. J. Cowell, T. M. Carpenter, J. R. Mclaughlan, A. A. Cubukcu, and S. Freear, "High-Frame-Rate Contrast-Enhanced Echocardiography Using Diverging Waves: 2-D Motion Estimation and Compensation," *IEEE Trans. Ultrason. Ferroelectr. Freq. Control*, vol. 66, no. 2, pp. 359–371, Feb. 2019, doi: 10.1109/TUFFC.2018.2887224.

[20] J. Voorneveld *et al.*, "High Frame Rate Contrast-Enhanced Ultrasound for Velocimetry in the Human Abdominal Aorta," *IEEE Trans. Ultrason. Ferroelectr. Freq. Control*, vol. 65, no. 12, pp. 2245–2254, 2018, doi: 10.1109/TUFFC.2018.2846416.

[21] J. Voorneveld *et al.*, "High-Frame-Rate Echo-Particle Image Velocimetry Can Measure the High-Velocity Diastolic Flow Patterns," *Circ. Cardiovasc. Imaging*, vol. 12, no. 4, Apr. 2019, doi: 10.1161/CIRCIMAGING.119.008856.

[22] A. Kheradvar *et al.*, "Echocardiographic Particle Image Velocimetry: A Novel Technique for Quantification of Left Ventricular Blood Vorticity Pattern," *J. Am. Soc. Echocardiogr.*, vol. 23, no. 1, pp. 86–94, Jan. 2010, doi: 10.1016/j.echo.2009.09.007.

[23] C. Prinz *et al.*, "Can echocardiographic particle image velocimetry correctly detect motion patterns as they occur in blood inside heart chambers? A validation study using moving phantoms," *Cardiovasc. Ultrasound*, vol. 10, no. 1, p. 24, Dec. 2012, doi: 10.1186/1476-7120-10-24.

[24] H. Gao, P. Claus, M. S. Amzulescu, I. Stankovic, J. D'Hooge, and J. U. Voigt, "How to optimize intracardiac blood flow tracking by echocardiographic particle image velocimetry? Exploring the influence of data acquisition using computer-generated data sets," *Eur. Heart J. Cardiovasc. Imaging*, vol. 13, no. 6, pp. 490–499, 2012, doi: 10.1093/ejechocard/jer285.

[25] C. Dietrich *et al.*, "How to perform Contrast-Enhanced Ultrasound (CEUS)," *Ultrasound Int. Open*, vol. 04, no. 01, pp. E2–E15, Jan. 2018, doi: 10.1055/s-0043-123931.

[26] M.-X. Tang *et al.*, "Quantitative contrast-enhanced ultrasound imaging: a review of sources of variability," *Interface Focus*, vol. 1, no. 4, pp. 520–539, Aug. 2011, doi: 10.1098/rsfs.2011.0026.

[27] C. Tremblay-Darveau, R. Williams, P. S. Sheeran, L. Milot, M. Bruce, and P. N. Burns, "Concepts and Tradeoffs in Velocity Estimation With Plane-Wave Contrast-Enhanced Doppler," *IEEE Trans. Ultrason. Ferroelectr. Freq. Control*, vol. 63, no. 11, pp. 1890–1905, Nov. 2016, doi: 10.1109/TUFFC.2016.2596581.

[28] M. Toulemonde, R. J. Eckersley, and M.-X. Tang, "High frame rate contrast enhanced echocardiography : Microbubbles stability and contrast evaluation," 2017.

[29] O. Couture, M. Fink, and M. Tanter, "Ultrasound contrast plane wave

imaging," *IEEE Trans. Ultrason. Ferroelectr. Freq. Control*, vol. 59, no. 12, pp. 2676–2683, 2012, doi: 10.1109/TUFFC.2012.2508.

[30] F. Scarano and M. L. Riethmuller, "Advances in iterative multigrid PIV image processing," *Exp. Fluids*, vol. 29, no. 7, pp. S051–S060, Dec. 2000, doi: 10.1007/s003480070007.

[31] B. Y. S. Yiu, S. S. M. Lai, and A. C. H. Yu, "Vector Projectile Imaging: Time-Resolved Dynamic Visualization of Complex Flow Patterns," *Ultrasound Med. Biol.*, vol. 40, no. 9, pp. 2295–2309, 2014, doi: 10.1016/j.ultrasmedbio.2014.03.014.

[32] J. Voorneveld *et al.*, "4-D Echo-Particle Image Velocimetry in a Left Ventricular Phantom," *Ultrasound Med. Biol.*, vol. 46, no. 3, pp. 805–817, Mar. 2020, doi: 10.1016/j.ultrasmedbio.2019.11.020.

[33] C. Tremblay-Darveau, R. Williams, L. Milot, M. Bruce, and P. N. Burns, "Combined perfusion and doppler imaging using plane-wave nonlinear detection and microbubble contrast agents," *IEEE Trans. Ultrason. Ferroelectr. Freq. Control*, vol. 61, no. 12, pp. 1988–2000, Dec. 2014, doi: 10.1109/TUFFC.2014.006573.

[34] L. Agati *et al.*, "Quantitative analysis of intraventricular blood flow dynamics by echocardiographic particle image velocimetry in patients with acute myocardial infarction at different stages of left ventricular dysfunction.," *Eur. Heart J. Cardiovasc. Imaging*, no. Lv, pp. 1–10, 2014, doi: 10.1093/ehjci/jeu106.

[35] S. Kutty *et al.*, "Effects of Right Ventricular Hemodynamic Burden on Intraventricular Flow in Tetralogy of Fallot: An Echocardiographic Contrast Particle Imaging Velocimetry Study," *J. Am. Soc. Echocardiogr.*, vol. 27, no. 12, pp. 1311–1318, 2014, doi: 10.1016/j.echo.2014.09.016.

[36] P. P. Sengupta *et al.*, "Left Ventricular Isovolumic Flow Sequence During Sinus and Paced Rhythms. New Insights From Use of High-Resolution Doppler and Ultrasonic Digital Particle Imaging Velocimetry," *J. Am. Coll. Cardiol.*, vol. 49, no. 8, pp. 899–908, 2007, doi: 10.1016/j.jacc.2006.07.075.

[37] H. Abe *et al.*, "Contrast echocardiography for assessing left ventricular vortex strength in heart failure: A prospective cohort study," *Eur. Heart J. Cardiovasc. Imaging*, vol. 14, no. 11, pp. 1049–1060, 2013, doi: 10.1093/ehjci/jet049.

[38] G. Goliasch *et al.*, "CRT improves LV filling dynamics: Insights from echocardiographic particle imaging velocimetry," *JACC Cardiovasc. Imaging*, vol. 6, no. 6, pp. 704–713, 2013, doi: 10.1016/j.jcmg.2013.04.004.

[39] G.-R. Hong *et al.*, "Characterization and quantification of vortex flow in the human left ventricle by contrast echocardiography using vector particle image velocimetry.," *JACC. Cardiovasc. Imaging*, vol. 1, no. 6, pp. 705–717, 2008, doi: 10.1016/j.jcmg.2008.06.008.

[40] R. Faludi *et al.*, "Left ventricular flow patterns in healthy subjects and patients with prosthetic mitral valves: An in vivo study using echocardiographic particle image velocimetry," *J. Thorac. Cardiovasc. Surg.*, vol. 139, no. 6, pp. 1501–1510, 2010, doi: 10.1016/j.jtcvs.2009.07.060.

[41] S. Fadnes, K. Sørensen, S. A. Nyrnes, M. S. Wigen, and L. Lovstakken, "Intraventricular Pressure Gradients - Vector Flow Imaging versus Color M-Mode," 2020.

[42] Y. Benito *et al.*, "Age-Dependence of Flow Homeostasis in the Left Ventricle," *Front. Physiol.*, vol. 10, no. APR, Apr. 2019, doi: 10.3389/fphys.2019.00485.

[43] L. Rossini *et al.*, "A clinical method for mapping and quantifying blood stasis in the left ventricle," *J. Biomech.*, vol. 49, no. 11, pp. 2152–2161, Jul. 2016, doi: 10.1016/j.jbiomech.2015.11.049.

Jason Voorneveld. was born in Johannesburg, South Africa, in 1987. He received the B.Sc. degree in electro-mechanical engineering and an M.Sc. degree in biomedical engineering from the University of Cape Town, Cape Town, South Africa, in 2009 and 2014, respectively. He obtained his Ph.D. degree in biomedical engineering at Erasmus MC, Rotterdam, The Netherlands in 2019.

He is currently working as a postdoc at Erasmus MC. His research interests include high-frame-rate ultrasound imaging, blood-flow imaging and contrast enhanced ultrasound imaging.

Lana B.H. Keijzer was born in Leiderdorp, the Netherlands, in 1992. She received the BSc and MSc. degrees in Applied Physics, with a specialization in medical and acoustical waveform imaging from the Delft University of Technology, Delft, the Netherlands, in 2013 and 2015 respectively. In 2016, she also received the MSc. degree in Management of Technology from the same university. In 2020, she obtained the PhD degree at the Department of Biomedical Engineering, Thorax Center, Erasmus Medical Center, Rotterdam, the Netherlands. Her thesis focusses on cardiac shear wave elastography measurements. She is currently working as a Clinical Physicist in training.

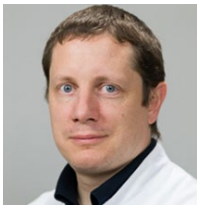

Mihai Strachinaru received his MD degree from the "Carol Davila" University of Medicine and Pharmacy, Bucharest, Romania in 2001 and his Cardiology specialization in 2008. He then moved on to work as a cardiologist in France (2008-2009), Belgium (2009-2016) and The Netherlands (2016-2019). During this period, he developed a keen interest in cardiac non-invasive imaging, especially echocardiography. He currently holds Romanian, French and European certifications in transthoracic and transesophageal echocardiography. In 2020 he received his PhD degree with the Department of Biomedical Engineering at Erasmus MC, Rotterdam, The Netherlands, for "Shear wave echocardiography". He is currently a postdoc researcher with the Erasmus MC and Intensive Care cardiologist in the CHIREC Hospital, Brussels, Belgium. His research interests include high frame rate ultrasound imaging in all its aspects: 2-D and 3-D, cardiac shear waves, ultrafast Doppler, contrast imaging, and related preclinical and clinical applications.

Daniel Bowen (1986) is a research echocardiographer based since 2018 in the Department of Cardiology at Erasmus MC, Rotterdam, The Netherlands. He trained in echocardiography at Papworth Hospital, Cambridge, UK (2014-2017) and beforehand at Colchester General Hospital (2010-14) following completion of a BSc degree in Clinical Physiology at Middlesex University, London (2013). He collaborates with the Department of Biomedical Engineering at Erasmus MC to aid the research and development of novel ultrasound modalities.

Ferit Onur Mutluer was born in Istanbul, Turkey in 1983. He received his MD degree from Hacettepe University Medical Faculty, Ankara, Turkey. He received his interventional cardiology training from Siyami Ersek Hospital, Istanbul. He is an associate professor in Istinye University, Istanbul and currently a Ph.D. candidate in Erasmus MC, Rotterdam, the Netherlands. His current research focuses on speckle tracking echocardiography, adult congenital heart disease and non-invasive flow visualization.

Antonius F. W. van der Steen (M'94–SM'03–F'13) received his M.Sc. (applied physics) from the Delft University of Technology in 1989, and a Ph.D. degree (medical sciences) from the University of Nijmegen in 1994. Since 1994 he is connected to the Thorax Centre, Erasmus MC Rotterdam. Since 2002, he is full Professor and the Head of Biomedical Engineering with Erasmus MC. Since 2013, he is full Professor of Applied Physics with the Delft University of Technology. Since 2013, he is also an honorary visiting Professor with the Chinese Academy of Sciences, Shenzhen Institute of Advanced Technologies. He is cofounder and past chairman of the Medical Delta: a collaboration between Erasmus MC, TU Delft and Leiden University Medical Centre, working on technical solutions for sustainable health.

He is member of the Netherlands Academy of Engineering (AcTI) and board member of the Netherlands Academy of Sciences (KNAW). He is Fellow of the IEEE and Fellow of the European Society of Cardiology. From 2014-2017 he was the Chairman of the board of the Dutch Technology foundation and of the NWO Technical Sciences. He was a recipient of the 2000 NWO PIONIER Technical Sciences and the 2007 Simon Stevin Master. He was the IEEE UFFC Distinguished lecturer 2011-2012. His expertise is mainly in diagnostic cardiologic imaging devices with emphasis on echography. Current research interests are focused to image guided catheter based treatment of atherosclerosis, ultrasound contrast agents, ultrasound transducers and vascular biomechanics.

Folkert J. Ten Cate was born in 1948. He graduated from Erasmus University Medical Center, Rotterdam, The Netherlands, as an M.D. in 1972 and defended his Ph.D. dissertation and became a Board Certified cardiologist in 1978. Since 1978, he has been a staff member of the Thoraxcenter, Erasmus Medical Center, Rotterdam – where his research focused the clinical applications of novel 2D and 3D ultrasound transducers. He was one of the first investigators worldwide who took an interest in microbubbles for contrast echocardiography. He has been a co-organizer for the European Symposium of Ultrasound Contrast Imaging in Rotterdam since 1996. In the last years his main interest has been in the research of micro bubbles for gene and drug delivery.

Nico de Jong (A'97–M'09) received his physics M.Sc. specialized in the field of pattern recognition from Delft University of Technology, Delft, The Netherlands, in 1978, and the Ph.D. in acoustic properties of ultrasound contrast agents in 1993 from the Department of Biomedical Engineering, Thorax Center, Erasmus MC, The Netherlands. In 2003, he joined the University of Twente, Enschede, the Netherlands, as a part-time Professor. He currently teaches with Technical Universities and Erasmus MC. He has been a Promotor of 21 Ph.D. students and is currently co-supervising 11 Ph.D. students. Since 1980, he has been a Staff Member with the Thorax Center, Erasmus Medical Center (Erasmus MC), Rotterdam, The Netherlands. Since 2011, he has been a Professor of Molecular Ultrasonic Imaging and Therapy with Erasmus MC and the Delft University of Technology, and since 2015, he has been the part-time Head of the Department of Acoustical Waveform Imaging with the Delft University of Technology. He is the Organizer of the Annual European Symposium on Ultrasound Contrast Imaging, Rotterdam. He is on the Safety Committee of the World Federation of *Ultrasound in Medicine and Biology*, and is an Associate Editor of Ultrasound in Medicine and Biology, and a Guest Editor of the special issues of different journals.

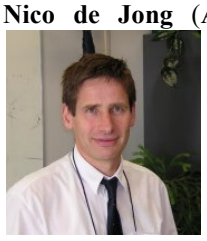

Hendrik J. Vos (M '14) received the M.Sc. degree in Applied Physics from Delft University of Technology, Delft, The Netherlands in 2004, and his Ph.D. degree with the Department of Biomedical Engineering at Erasmus MC, Rotterdam, The Netherlands, in 2010. He worked as a Postmaster Researcher with the University of Florence, Italy, and as a contract researcher for the petrochemical industry on cutting-edge ultrasonic solutions. He currently is associate professor with Erasmus MC, and received a Dutch NWO-TTW-VIDI personal grant in 2018. His research interests include acoustical array technology for biomedical imaging in all its aspects: transducers, 2-D and 3-D beamforming, cardiac shear waves,

ultrafast Doppler, contrast imaging, and related subclinical and clinical studies.

Annemien van den Bosch is a cardiologist at the Erasmus University Medical Centre in Rotterdam, The Netherlands. Her clinical work and research involves adult congenital heart disease, echocardiography and pulmonary hypertension. She is also involved in basic and translational research on new echocardiographic techniques as high frame rate echocardiography, the development of multi-plane echocardiography and the value of imaging biomarkers in the follow-up of patients with congenital heart disease.

Johan G. Bosch received the M.Sc. degree in Electrical Engineering from Eindhoven University of Technology, Eindhoven, The Netherlands, in 1985, and the Ph.D. degree from Leiden University Medical Center, Leiden, The Netherlands, in 2006. He is currently an Associate Professor and a Staff Member with Thoraxcenter Biomedical Engineering, Department of Cardiology, Erasmus University Medical Center Rotterdam, Rotterdam, The Netherlands. He is a (Co-)PI of projects on 3-D ultrasound image formation, transducer development, 2-D and 3-D cardiovascular imaging, flow and tissue stiffness assessment using novel ultrasound approaches. His research interests include echocardiographic image processing, transducer development, and novel ultrasound techniques for image formation and functional imaging.